UNIVERSITY OF LEEDS

This is a repository copy of *Investigation of Electromagnetic Mode Transition and Filtering of an Asymptotically Single-mode Hollow THz Bragg Fibre*.

White Rose Research Online URL for this paper:
http://eprints.whiterose.ac.uk/131984/

Version: Accepted Version

Article:
Hong, B orcid.org/0000-0002-8033-5438, Chudpooti, N, Akkaraekthalin, P et al. (3 more authors) (2018) Investigation of Electromagnetic Mode Transition and Filtering of an Asymptotically Single-mode Hollow THz Bragg Fibre. Journal of Physics D: Applied Physics, 51 (30). ARTN 305101. ISSN 0022-3727

https://doi.org/10.1088/1361-6463/aaccaa

(c) 2018 IOP Publishing Ltd. This is an author produced version of a paper published in Journal of Physics D: Applied Physics. Uploaded in accordance with the publisher's self-archiving policy.

Reuse
Items deposited in White Rose Research Online are protected by copyright, with all rights reserved unless indicated otherwise. They may be downloaded and/or printed for private study, or other acts as permitted by national copyright laws. The publisher or other rights holders may allow further reproduction and re-use of the full text version. This is indicated by the licence information on the White Rose Research Online record for the item.

Takedown
If you consider content in White Rose Research Online to be in breach of UK law, please notify us by emailing eprints@whiterose.ac.uk including the URL of the record and the reason for the withdrawal request.

White Rose university consortium
Universities of Leeds, Sheffield & York

eprints@whiterose.ac.uk
https://eprints.whiterose.ac.uk/

Investigation of Electromagnetic Mode Transition and Filtering of an Asymptotically Single-mode Hollow THz Bragg Fibre

Binbin Hong[1*], Nonchanutt Chudpooti[1,2], Prayoot Akkaraekthalin[2], Nutapong Somjit[1], John Cunningham[1], and Ian Robertson[1]

1. School of Electronic and Electrical Engineering, University of Leeds, Leeds LS2 9JT, UK
2. Department of Electrical and Computer Engineering, King Mongkut's University of Technology North Bangkok, Bangkok 10800, Thailand

E-mail: *elbho@leeds.ac.uk

Abstract

The mechanism for electromagnetic (EM) mode transition and filtering in an asymptotically single-HE_{11}-mode hollow THz Bragg fibre is investigated. We designed, fabricated, and measured Bragg fibres with an asymptotically single-mode pattern, achieving measured signal propagation loss of better than 3 dB/m at 0.265 THz and with an operating frequency range from 0.246 to 0.276 THz. Mode transition and filtering effects are both verified by 3D full-wave simulations using measured material properties, with geometrical parameters extracted from the fabricated Bragg fibre prototypes. By optimizing the coupling efficiency between the free-space Gaussian beam and the guided Bessel function mode, the optimum distance of mode transition from the Gaussian-beam excitation into the guided mode is calculated to be ~13.7 free-space wavelengths in our fibre, to ensure fast EM-field convergence to the desired asymptotically single-mode mode pattern in the Bragg fibre. After this mode transition region, the electric field amplitude ratio between the desired HE_{11} mode and the main competing HE_{12} mode is approximately 7 times, with the HE_{12} mode attenuation being more than 10 dB/m larger than the fundamental HE_{11} mode; the results indicate that our fibre is one of the best candidates for low-loss asymptotically single-mode terahertz signal interconnections.

Keywords: Bragg fibre, electromagnetic propagation, single-mode, mode transition, modal-filtering effect

1. Introduction

Low-loss and single-mode THz waveguides are vital interconnects between different functional components in THz systems. The requirement of low propagation loss has seen recent developments in hollow THz waveguides, such as Bragg fibres [1-3], hexagonal photonic crystal fibres [4,5], tube-lattice fibres [6 , 7], dielectric tubes [8 , 9], and metal-coated dielectric tubes [10 , 11]. To minimise the propagation loss and group velocity dispersion, the above-mentioned THz waveguides generally operate in a highly multimode regime, resulting in mode competition problems [12]. A modal-filtering effect [13-15], achievable by exploiting loss-discrimination between the nominal operating mode and other competing modes, can allow such waveguides to operate in an asymptotically single-mode pattern, however.

In asymptotically single-mode THz waveguides, a certain propagation distance is required to ensure the transition from multimode operating pattern to the effectively single-mode pattern. However, most previously published works on THz waveguides [1-14] only focus on the steady state of the supported propagating modes in the fibre. A rigorous investigation of the EM-field mode transition and filtering processes prior to steady-state propagation is largely lacking. Specifically, it is essential to know the mode transition distance since this determines whether the THz waveguide is suitable for certain applications. For example, due to the small loss discrimination between the desired mode and the unwanted modes, the conventional design principles [15-17] for optical Bragg fibre require several kilometres to eliminate the unwanted modes, and are therefore unsuitable for THz Bragg fibres, which are mainly considered in applications that require much shorter waveguiding distance, such as biological and security imaging [18,19].

In this paper, we investigate the mode transition and filtering phenomenon by using a 3D full-wave simulation of the EM wave propagation inside and along the length of a hollow all-polymer THz Bragg fibre, using directly measured material dielectric properties and with real geometric parameters [2]. The THz Bragg fibre discussed here can achieve asymptotical single-mode pattern propagation with large loss discrimination between the fundamental and other higher-order modes. Two different excitation methods (waveguide-port excitation and Gaussian-beam excitation) are considered in our full-wave simulations, representing multimode excitation and quasi-single mode excitation conditions, respectively. Using a multimode waveguide port

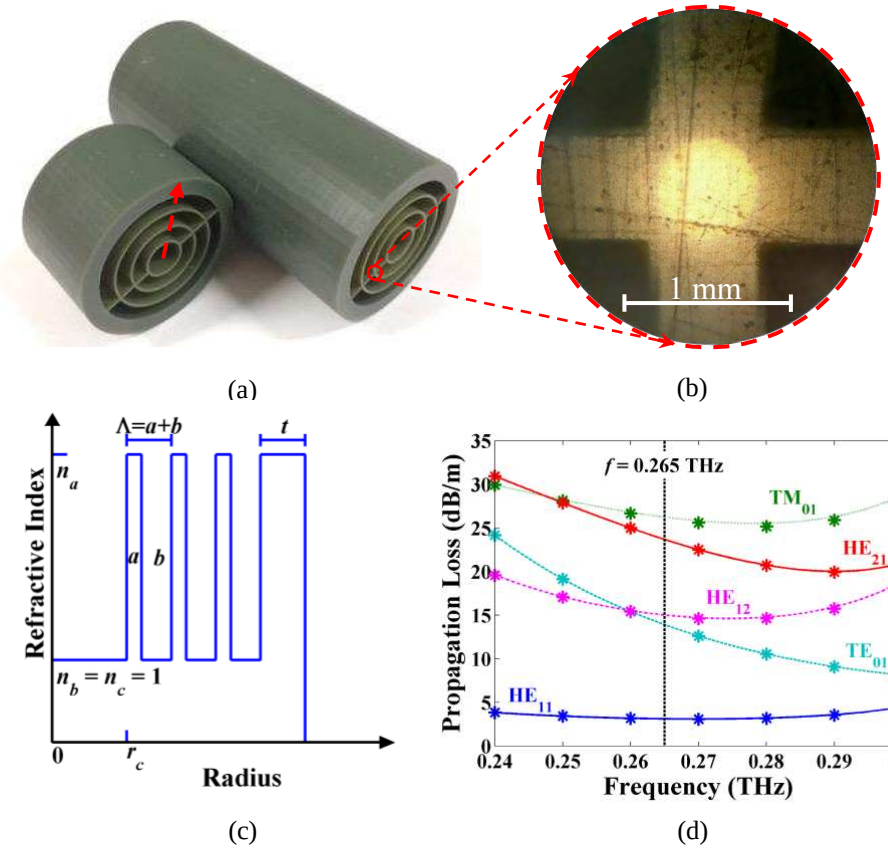

Figure 1. The hollow THz Bragg fibre in this work. (a) The fabricated Bragg fibre prototypes; (b) The zoomed view of the fibre at the junction of the dielectric layer and the support bridges; (c) The radial refractive index profile of the Bragg fibre along the red dashed arrow in (a). (d) Calculated (lines) and numerically simulated (asterisks) propagation losses of selected lowest-loss supported propagating modes in the fibre without support bridges. Here, $n_a = 1.644 + 0.0293i$, $n_b = n_c = 1$, $a = 0.667$ mm, $b = 3.877$ mm, $r_c = 4681$ mm, $t = 4.544$ mm, and the width of the support bridges is $w = 0.652$ mm.

excitation method, the filtering of different high-order modes, which correspond to different radiation angles, is clearly observed, indicating a good mode selectivity of the proposed Bragg fibre. With appropriate Gaussian-beam excitation, most high-order competing modes can be quickly and effectively filtered out after a distance of approximately 13.7 free-space wavelengths, and beyond this point, the electric field amplitude of the desired HE_{11} mode is observed to be approximately 7 times larger than the main competing HE_{12} mode's. Additionally, the propagation loss of the HE_{12} mode is more than 10 dB/m higher than that of the fundamental HE_{11} mode. Therefore, the asymptotically single-mode propagation of the desired operational mode can be formed inside the fibre. The simulated propagation loss of the Bragg fibre is approximately 5 dB/m, which is in a good agreement with the experimental result of 3 dB/m, recently published by the authors [2].

2. Design of the fibre

Figs. 1 (a) and (c) shows the geometry and refractive index profile of the fabricated all-polymer Bragg fibre prototype. The Fig. 1 (b) shows the zoomed view of the fibre taken by using an optical microscope. The dents on the surface of the fibre shown in the figure are much narrower than the free-space waveguide at the central operating frequency, namely 1.131 mm at 0.265 GHz, and thereby they are believed to have negligible impact on the performance of the fibre. The Bragg fibre consists of an air core ($n_c = 1$) cladded by periodic concentric dielectric layers of alternatively high (n_a) and low (n_b) refractive index materials, the thickness of which are a and b respectively, while r_c is the core radius and $\Lambda = a + b$ is the period of the radial photonic crystal. The outermost layer is a thick protective polymer layer which absorbs residual outgoing EM waves and isolates the fibre from external perturbation. The thickness of the outermost layer is t, while the width of the support bridges which mechanically support the air gap between concentric rings is w.

The design principles of the fabricated Bragg fibre were reported in our previous works [13, 20] and is briefly

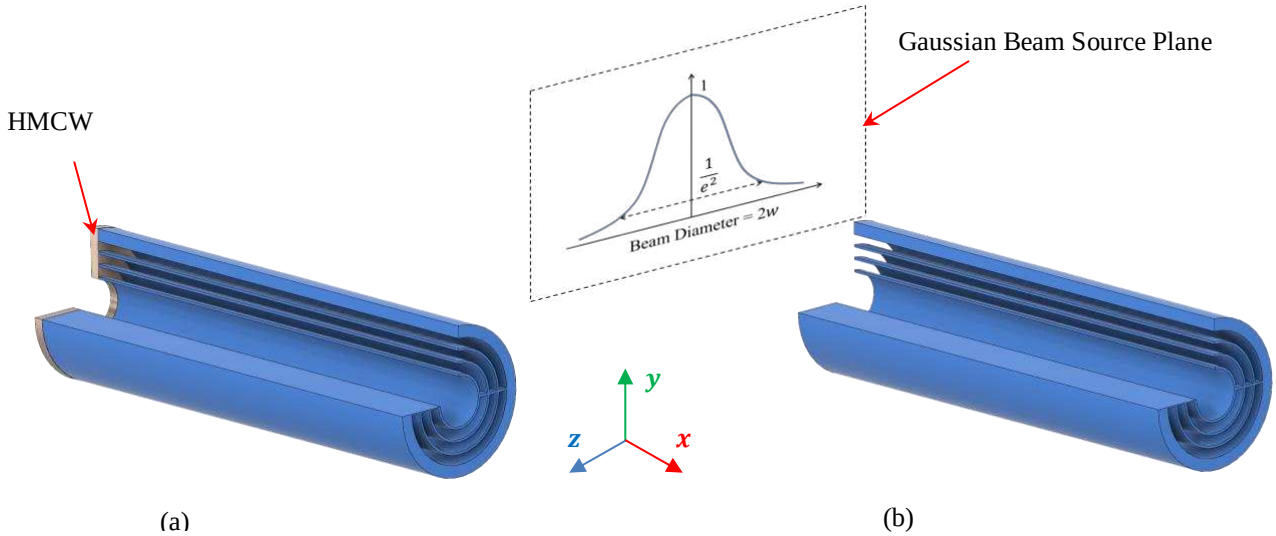

Figure 2. Cutaway views of the proposed Bragg fibre for CST simulation using different excitation schemes. (a) Hollow cylindrical metallic waveguide excitation scheme. The core radius of HMCW is the same as the core radius of the Bragg fibre, namely 4.681 mm. The length of the HMCW is 1.131 mm. (b) Gaussian beam excitation scheme. The distance between the source plane and the input port of the Bragg fibre is 25.4 mm. The focal length and the beam waist of the Gaussian beam are 25.4 mm and 3.604 mm, respectively. The length of the Bragg fibre in both (a) and (b) is 125 mm. The origins of the coordinate in both schemes are placed at the centre of input port of the Bragg fibre.

summarized as follows: 1) Among several available photopolyers for the EnvisionTEC Perfactory 3 Mini 3D printer, HTM140 is chosen as the material for the high refractive index regions for the proposed hollow-core single-polymer Bragg fibre due to its relatively high refractive index and low material loss. 2) The values of a and b are subsequently chosen based on a generalized half-wavelength condition [13] to provide a wide photonic bandgap centred around 0.27 THz which covers the frequency of interest. 3) The core radius r_c is carefully chosen to place the dispersion curve of the desired HE_{11} mode in the low confinement loss photonic bandgap region. 4) Both the width of the support bridges w and the thickness of the outermost protective layer t have little influence on the performance of the proposed high-porosity Bragg fibre, and they are chosen based on simulation optimization results. Here, the 3D printing technique that was used to fabricate the proposed Bragg fibre employs digital light processing technology, which is cost-effective, fast and convenient to fabricate high-porosity air-core Bragg fibre. However, it is challenging to fabricate extreme thin dielectric layer and long fibre using this technique, mainly limited by the printing resolution and the overall building space of the 3D printer. The complex refractive index of HTM140 used in this paper is based on the measurement results shown in [2].

Using a transfer matrix method [21, 22], the propogation losses of the several selected lowest-loss supported modes of the fabricated Bragg fibre can be calculated analytically. The analytical results (lines) based on the transfer matrix method with the simulation results (asterisks) based on COMSOL are shown in Fig. 1 (d). The HE_{11} mode is selected as the fundamental mode as it has the lowest propagation loss over the frequency range from 0.24 to 0.3 THz. Since the HE_{11} mode is a linearly polarized mode which can barely couple with the circularly polarized TE_{01} mode, the main competing mode of HE_{11} is thus HE_{12} rather than TE_{01}. The minimum loss discrimination between the HE_{11} and HE_{12} modes over the frequencies of interest occurs at 0.265 THz, where they show a difference in their propagation loss of approximately 10 dB/m. As the only artificially engineered material, the mateiral properties of HTM140 could potentially affect the performance of the fibre, if the complex refractive index of HTM140 varies significantly over the operating frequency range and has a large uncertainty about the exactly value of the complex refractive index. According to the measuremnd result shown in [2], the difference between the measured results and the fitted data for the refractive index and extinction coefficnet is up to 0.009 and 0.012, respectively. According to our theoretically analysis, the uncertainty of the complex refractive index of HTM140 contributes up to 0.005% and 0.025% variances of the dispersion curves of HE_{11} and HE_{12}, respectively, and also contributes up to 15% and 12% variances of the propagation loss of HE_{11} and HE_{12}, respectively. Therefore, the impact of the refractive index uncertainty on the perfermances of the fibre, e.g. the dispersion relation and the propagation loss, is reasonable small, and is believed to be negligible.

3. 3D Full-wave EM simulation

Unlike standard hollow metallic rectangular or circular waveguides, the Bragg fibre is a non-standard waveguide structure which, in practice, requires signal feeding from the

other types of waveguide port or from free-space signal sources. In this work, we consider two different excitation methods, conventional waveguide-port excitation and Gaussian-beam excitation, as shown in Fig. 2.

3.1. Multi-mode hollow cylindrical metallic waveguide excitation

From Fig. 1(d), at the operational frequency of 0.265 THz, the propagation loss of the HE_{11} mode is lowest. Moreover, the loss discrimination between the HE_{11} mode and the HE_{12} mode is highest as compared to the other frequencies in the operational bandwidth of 0.24 to 0.3 THz. Therefore, we choose to analyze the fibre at 0.265THz, as indicated by the vertical dashed line in the figure. The 3D full-wave model of the proposed Bragg fibre using the measured geometrical parameters and material dielectric properties, shown in Fig. 2 (a), is simulated using the CST Studio Suite®. All boundaries are set as radiation boundaries in order to absorb any

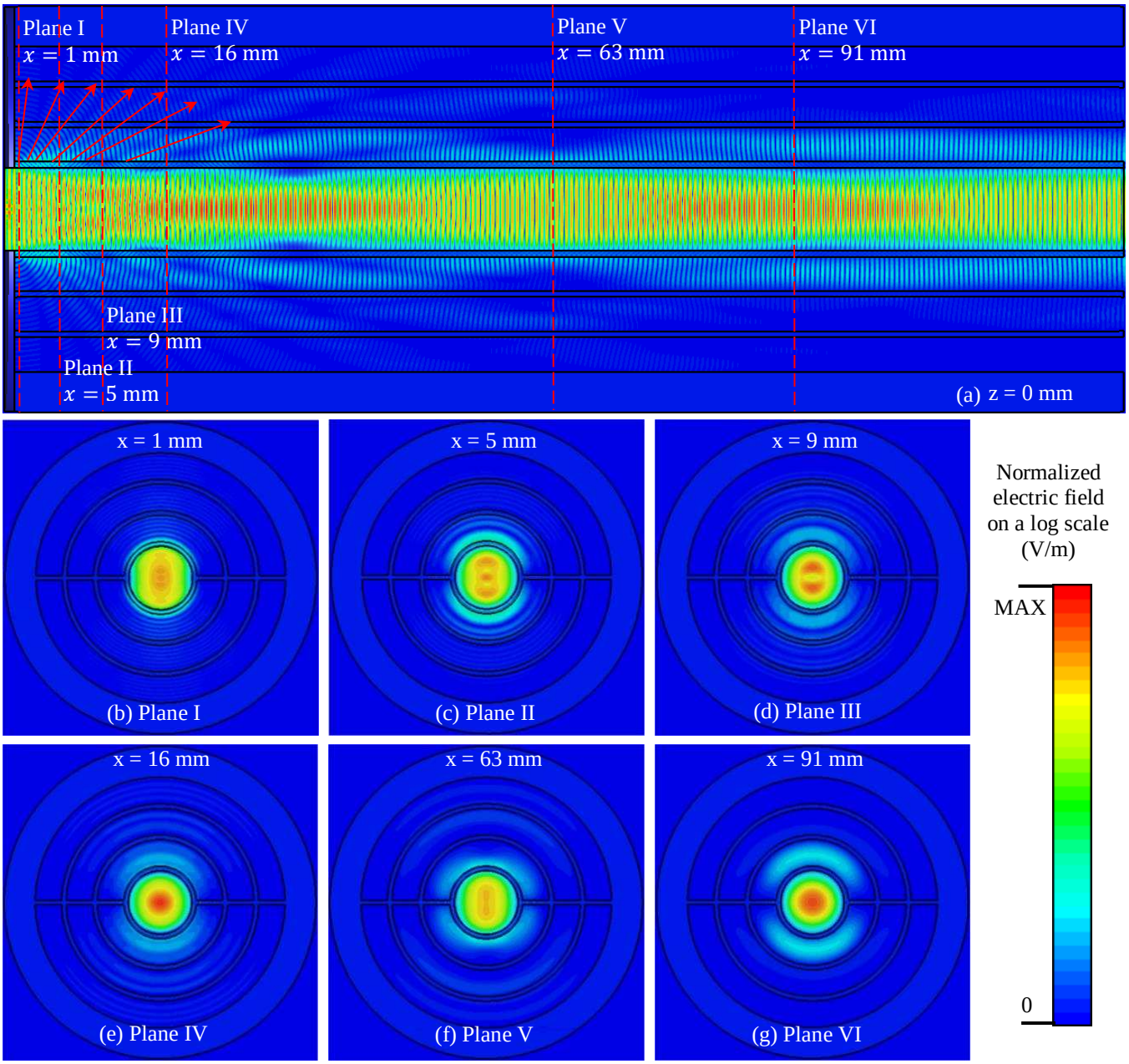

Figure 3. Absolute electric field with HMCW excitation at 0.265 THz using a log scale colour map. The coordinate scheme is the same as that in Fig. 2. (a) $z = 0$ mm plane. Vertical dashed lines represent the positions of different transverse cut planes. Solid red arrows represent the different radiation angles of the electromagnetic field which correspond to different modes. (b) Plane I ($x = 1$ mm). (c) Plane II ($x = 5$ mm). (d) Plane III ($x = 9$ mm). (e) Plane IV ($x = 16$ mm). (f) Plane V ($x = 63$ mm). (g) Plane VI ($x = 91$ mm).

outgoing EM waves preventing the reflection of EM waves at the boudnaries. A hollow metallic circular waveguide (HMCW) is used to excite an EM field at $x = 0$ mm. The core radius the feeding waveguide $r_m = r_c = 4.681$ mm, and its length $l_m = 1.131$ mm which is the same as the free-space wavelength λ_0 at 0.265 THz. Given the operating frequency f, the criteria allowing a HMCW to work in single-mode pattern is [23]

$$\frac{c}{3.41f} < r < \frac{c}{2.62f}$$

where c is the speed of light and r is the core radius. If $f = 0.265$ THz, then the criteria becomes 0.332 mm $< r < 0.432$ mm. Since the core radius of the feeding waveguide $r_m = 4.681$ mm $\gg 0.432$ mm, the feeding waveguide is highly multimode. Therefore, at the end of the feeding waveguide, the output field pattern is a superposition mode composed from many supported modes. Using a multimode excitation scheme allows better understanding of the filtering of higher-order competing modes in the proposed Bragg fibre.

The absolute electric field at 0.265 THz at the $z = 0$ plane, one of the longitudinal symmetry planes of the fibre, is shown in Fig. 3 (a). Overall, the EM field is substantially confined to the core of the fibre. However, the fibre does not work in a strictly single-mode pattern, requiring a certain distance before a relatively steady asymptotically single-mode state is obtained. We divide the fibre into two zones, as shown in Fig. 3 (a).

In zone I, which extends between 0 mm $\leq x \leq$ 16 mm ($0 \leq x \leq 14.1\lambda_0$), the EM modes transition from HMCW multi-modes to Bragg fibre modes. In this region, several radiation angles can be clearly observed, indicating a relatively strong radiation of electromagnetic field from the air core to the cladding layers. The radiation angles correspond to different supported propagating modes in the Bragg fibre; they are mainly lossy high-order competing modes. Figs. 3(b)–(g) show the transverse mode patterns of several representative points. In zone I, Figs. 3 (b)–(e), the gradual changes of the guided mode from a highly superposition mode to a relatively pure HE_{11} mode is achieved. Most higher-order competing modes are filtered out in this zone, allowing the Bragg fibre to operate in a relatively pure EM mode pattern thereafter. However, due to the relatively low loss among the competing modes, a small portion of the main competing mode HE_{12} may still exist in the fibre; it will also be gradually filtered out in the next zone by a modal-filtering effect.

In zone II, for $x \geq 16$ mm ($x \geq 14.1\lambda_0$), a periodic pattern with a period of approximately 61 mm or $53.9\lambda_0$ is observed. This periodic pattern is caused by mode-beating [24,25], from the interference between two modes of slightly different propagation constant. In our case, the two modes are the desired HE_{11} mode and its main competing mode HE_{12}. Fig. 3(f) and (g) show the mode pattern at one representative peak and valley, corresponding to the situation when the two modes are approximately in phase and 180 degrees out of phase, respectively. Fig. 3(f) shows that at the valley, the overall mode pattern behaves similarly to the desired HE_{11} mode, though the slight distortion of the mode pattern also indicates the existence of a small portion of the competing mode. Fig. 3 (g) shows clearly the mode pattern of HE_{11} at the beat peak. The residual competing mode in zone II can be gradually filtered out from the fibre by propagation loss, allowing the Bragg fibre to be operated in asymptotically single-mode pattern in this zone and beyond.

3.2. Single-mode free-space Gaussian excitation

Like conventional optical fibre and other hollow core THz microstructure fibres [26-28], Bragg fibres can be excited using a focused Gaussian beam. The EM mode transitions from the free-space Gaussian mode into a guided Bessel-function mode within the Bragg fibre. The mode transition process is closely related to the mode coupling at the input port. An efficient input coupling leads to a smooth mode transition process, consequently reducing the overall losses of the fibre [28, 29].

As the mode pattern of the desired HE_{11} mode in the Bragg fibre is similar to that of the TE_{11} mode in HMCW. The mode-coupling theory [30, 31], which describes the coupling coefficient of TE_{11} mode in HMCW when excited by a Gaussian beam can be used to estimate the efficiency of coupling from free-space Gaussian beam into the Bragg fibre, as shown in Fig. 4. When the ratio of the Gaussian beam waist to the core radius w_0/r_c is equal to 0.77, the

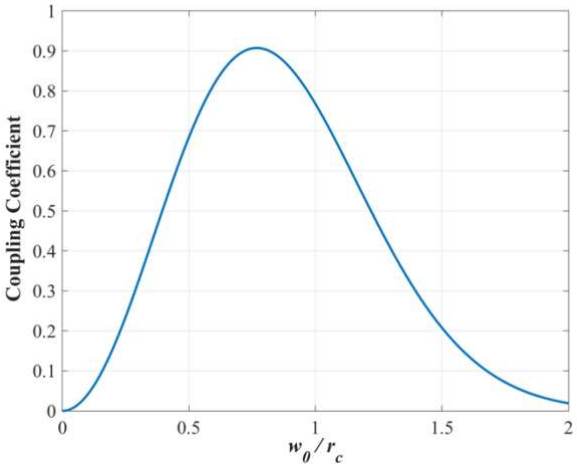

Figure 4. Calculated coupling coefficient between the free-space Gaussian beam and the HE_{11} mode in the proposed Bragg fibre, assuming the mode pattern of the HE_{11} mode in Bragg fibre is the same as that of the TE_{11} mode in HMCW.

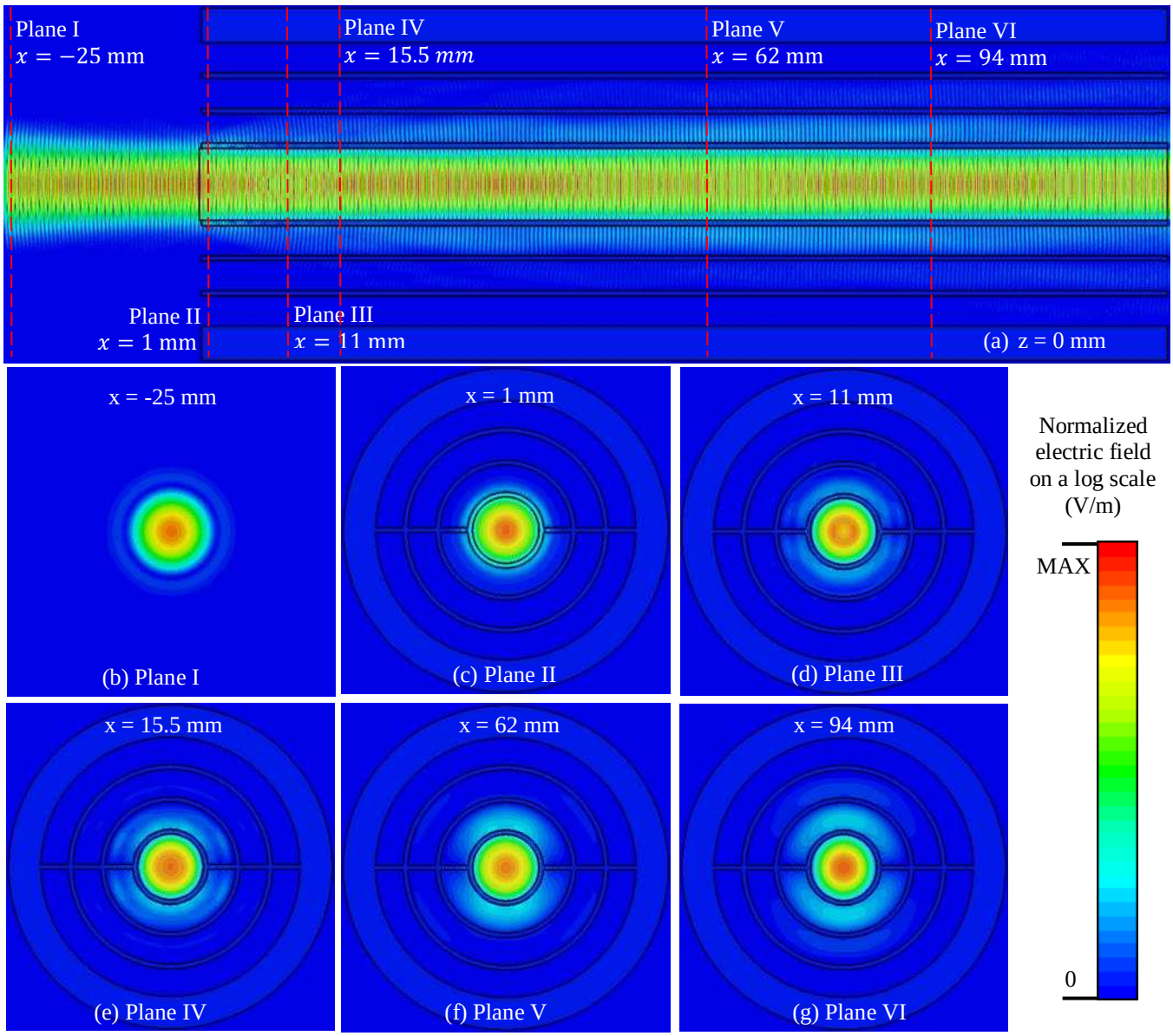

Figure 5. Absolute electric field with focused Gaussian beam excitation at 0.265 THz using log scale colour map. The Gaussian beam is excited at the $x = -25.4$ mm plane and focused at the input port of the fibre with a beam width at beam waist $w_0 = r_c$. The coordinate scheme is the same in Fig. 2. (a) $z = 0$ mm plane. (b) Plane I ($x = -25$ mm). (c) Plane II ($x = 1$ mm). (d) Plane III ($x = 11$ mm). (e) Plane IV ($x = 15.5$). (f) Plane V ($x = 62$ mm). (g) Plane VI ($x = 94$ mm).

coupling coefficient is as high as 90%. This ratio can be also used to maximize the coupling coefficient of the HE_{11} mode in Bragg fibre, as well as to suppress the coupling of Gaussian beam to other competing modes.

Since the core radius of the Bragg fibre $r_c = 4.681$ mm, a Gaussian beam waist $w_0 = 0.77r_c = 3.604$ mm is set in the full-wave simulation to maximise the coupling coefficient. The absolute electric field at the operating frequency of 0.265 THz at the $z = 0$ mm plane is shown in Fig. 5 (a), while Figs. 5 (b)–(g) show the transverse mode patterns at several representative points. From Fig. 5, when using free-space Gaussian beam as the feeding source (Plane I), the mode pattern at the input port of the fibre (Plane II) is relatively pure and close to the mode pattern of the desired HE_{11} mode. Additionally, compared with the strong radiation of electromagnetic field at the input of the fibre in the previous excitation scheme using HMCW, the radiation of the wave at the same part of the fibre in this excitation scheme is much weaker, and only very few radiation angles are observed. However, due to the impedance mismatch at the input interface of the fibre, a small amount of EM energy of the main competing mode HE_{12} is excited and causes a slight distortion on the overall mode pattern at Plane III, but the mode pattern quickly converges to the HE_{11} mode at $x =$

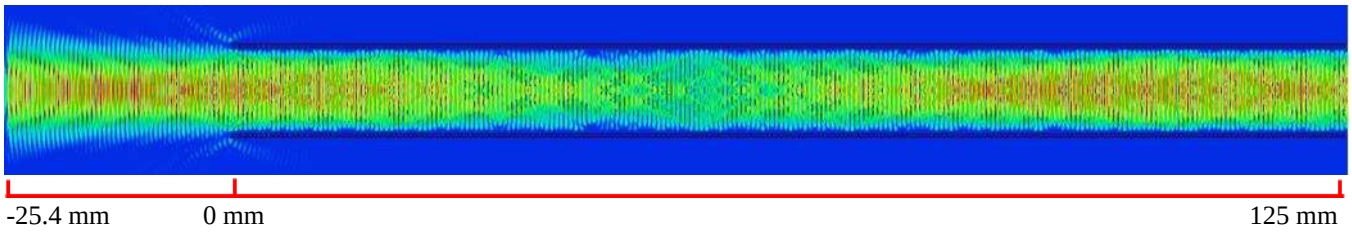

Figure 6. Absolute electric field of the electromagnetic field propagating in HMCW at $z = 0$ mm plane at 0.265 Hz. The core radius of the HMCW is 4.681 mm. The Guassian beam excitation source is placed at $x = -25.4$ mm. The parameters for the Gaussian beam are the same as those in fig. 5 (a).

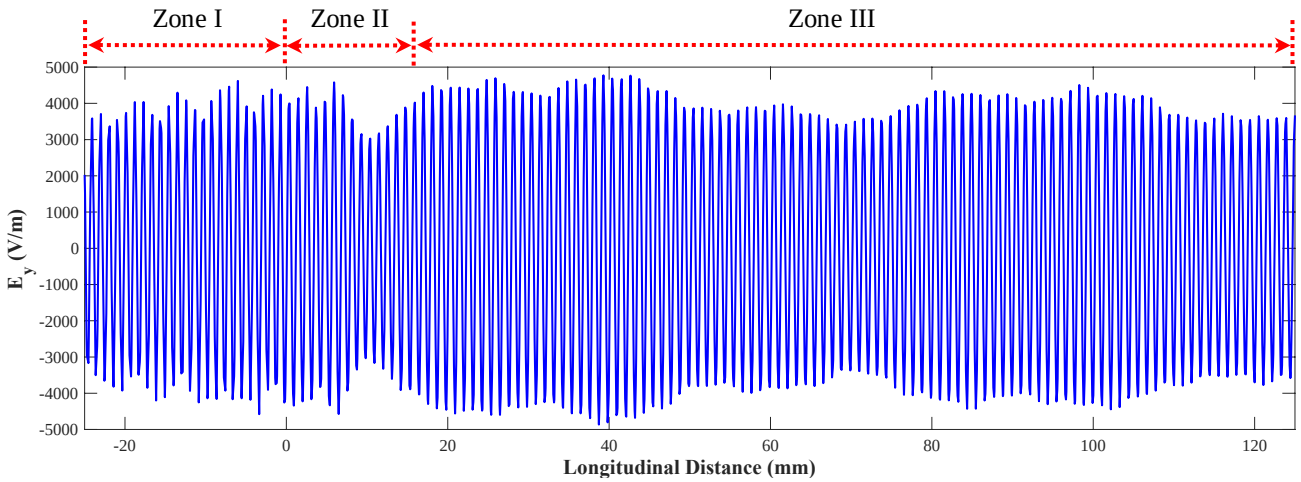

Figure 7. Plot of E_y along the x-axis of the fibre. In zone I (-25.4 mm $\leq x \leq 0$ mm), the wave travels in free space. Zone II (0 mm $\leq x \leq 15.5\ mm$) is a mode transition region where the free-space Gaussian beam transitions into a Bessel function. In zone III (15.5 mm $\leq x \leq 125\ mm$), the proposed Bragg fibre operates in an asymptotically single-mode pattern.

$15.5\ mm$ (Plane IV), which is approximately $13.7\lambda_0$. After this point, although the phenomenon of mode beating also exists, the amplitude of the mode beat is relatively weak, compared with the previous multi-mode excitation scheme using HMCW. Besides, the mode pattern at the beat valley (Plane V) is still well maintained as the desired HE_{11} mode and we can barely observe the distortion caused by the HE_{12} mode, suggesting that the amplitude of the competing HE_{12} mode is much weaker than that of the desired HE_{11} mode.

Therefore, compared with the previous excitation scheme using HMCW, the excitation scheme using a proper Gaussian beam in this design can lead to a better mode transition process and a shorter transition distance, and the fibre can operate in effectively asymptotically single-mode pattern after the transition point at around 13.7 operating wavelengths. When comparing the Bragg fibre with a conventional HMCW which uses the same radius as the air core, the single mode selection in Bragg fibre is much more obvious. Fig. 6 shows the EM-wave propagation in HMCW with Gaussian beam source excited from the left. The mode pattern in the HMCW is highly multimode, while, under the same excitation condition, the Bragg fibre works in effectively asymptotically single-mode pattern.

4. Mode Competing and filtering

4.1. Mode beat

When two competing modes with slightly different propagation constants simultaneously exist in the Bragg fibre, a periodic variation in the amplitude of the electric field can be observed, which is also known as mode beating [32]. Considering two EM waves of significantly different amplitudes added together linearly:

$$A\cos(2\pi\xi_1 x) + B\cos(2\pi\xi_2 x) = (A-B)\cos(2\pi\xi_1 x) + 2B\cos(2\pi\frac{\xi_1+\xi_2}{2}x)\cos(2\pi\frac{\xi_1-\xi_2}{2}x) \quad (1)$$

Here, A and B are the amplitudes of the two waves, where $A \gg B$. $\xi_n = 1/\lambda_{gn} = \beta_n/2\pi\ (n \in \mathbf{N})$ is the spatial frequency of a wave, where n is an identifier associated with different waves, λ_g is the guide wavelength and β is the longitudinal wave propagation number. ξ_1 and ξ_2 are quite close to each other. In the second term of the right side of eqn. (1), the frequency $(\xi_1 - \xi_2)/2$ is perceived as a periodic variation in the amplitude of the tone $(\xi_1 + \xi_2)/2$. In

addition, since $A \gg B$, the overall amplitude of the superposition mode is mainly dominated by the first term of the right side of the equation (1), while beat amplitude is mainly dominated by the second term.

To quantitatively understand the mode competition in the Bragg fibre, based on Fig. 5 (a), we plot E_y along the x-axis of the fibre in Fig. 7. x ranges from -25 mm to 125 mm, with a step size of 0.25 mm, which is about 22% of the guide wavelength of the HE_{11} mode, making it an appropriate step size to observe the high-frequency changes within one wavelength. In zone I, the wave propagates in the free-space region. In zone II, the free-space Gaussian beam transitions into Bessel function modes supported by the Bragg fibre. A sharp reduction of the amplitude of E_y at around $x = 11$mm or $x = 9.7\lambda_0$ is mainly attributed to the rapid increase of the higher-order competing modes due to the structure discontinuity at the input port of the fibre. In zone III, the amplitude of E_y varies periodically and decays as a result of both mode beating and propagation loss. The amplitude of the envelope for the beat is relatively small, however, compared with the amplitude of the signal.

To compare the EM-field strength of the main HE_{11} mode and its competing mode in zone III, we use a discrete Fourier transform to transform the E_y signal in zone III from the spatial domain to the spatial-frequency domain (Fig. 8). The spatial spectrum is relatively clean compared to that of the multimode excitation method, indicating a good mode selectivity of the Bragg fibre. The main peak at 894.5 m^{-1} corresponds to the desired HE_{11} mode. The secondary peak at 848.9 m^{-1} corresponds to the main competing HE_{12} mode. The amplitude of the main peak is about 7 times of the amplitude of the secondary peak. This agrees well with the previous analyses as in eqn. (1) and Fig. 7. The superposition of HE_{11} and HE_{12} creates the mode beating in zone III, and the overall amplitude of the signal in zone III is dominated by

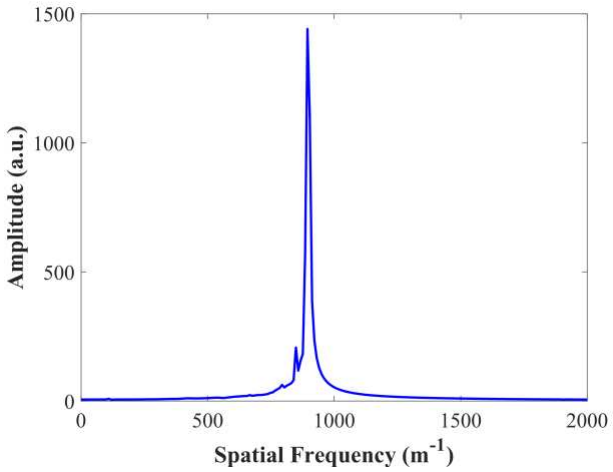

Figure 8. Discrete Fourier transform of the E_y signal in zone III of fig. 7.

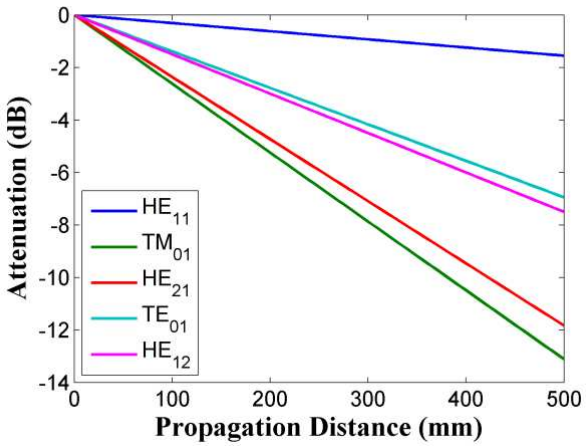

Figure 9. The attenuation of the desired HE_{11} mode and its main competing modes as a function of the propagation distance at 0.265 THz.

the desired HE_{11} mode, while the HE_{12} mode dominates the amplitude of the envelope of the beat. The large differences between the amplitudes and the propagation losses of the desired mode HE_{11} and the main competing mode HE_{12} allow the fibre to operate in effectively asymptotically single-mode pattern in zone III.

Based on the cut-back method by comparing the amplitude of E_y at the start ($x = 15.5$ mm) and the end ($x = 125$ mm) of the zone III, the propagation loss of the fibre is estimated to be 4.78 dB/m, which is comparable to the experimental result of 3 dB/m in our previous experimental work [2].

4.2. Mode filtering

In addition to the significant differences of the amplitude of the electromagnetic fields between the desired HE_{11} mode and its competing modes when the fibre has an efficient Gaussian-beam excitation source, substantial differences in the attenuation rate between fundamental HE_{11} and higher-order modes also contribute to the mode selection, creating a modal-filtering effect. Based on the theoretical results shown in Fig. 1(d), Fig. 9 shows the attenuation of the HE_{11} mode and its competing modes as a function of the propagation distance. At the distance of 200 mm, the power of the main competing mode HE_{12} drops by one half (-3 dB), while the attenuation of the HE_{11} mode is only 0.62 dB, and the difference of the propagation loss of these two modes is as large as 10 dB/m. Therefore, significant differences in the amplitude and the attenuation rate between the HE_{11} mode and its competing modes allow the fibre to operate in effectively asymptotically single-mode pattern with low propagation loss.

5. CONCLUSION

In this paper, 3D full-wave simulations have been used to study the mode transition and filtering in an asymptotically single-mode hollow THz Bragg fibre. The Bragg fibre was designed to support asymptotically single-mode operation centred at 0.265 THz. With multimode excitation using HMCW, good suppression of the higher-order competing modes was observed in the mode transition zone of the fibre. Using a Gaussian beam excitation source, a smoother and shorter transition zone was achieved, which is highly desirable in practical applications. The phenomenon of mode beating, caused by the superposition of the desired HE_{11} mode and its main competing mode HE_{12}, was also observed. However, due to the large discrimination between the amplitudes and the propagation losses of the modes, the proposed Bragg fibre can still operate in an effectively asymptotically single-mode pattern, making it a strong candidate as a low-loss interconnects for THz systems.

ACKNOELEDGEMENTS

This work has been supported by the China Scholarship Council, the Thailand Research Fund through the TRF Senior Research Scholar Program with Grant No.RTA6080008 and the Royal Golden Jubilee Ph.D. Program with Grant No.PHD/0093/2557. The data associated with this paper are openly available from the University of Leeds repository [33].

REFERENCE

[1] Dupuis, A., Stoeffler, K., Ung, B., Dubois, C. and Skorobogatiy, M., 2011. Transmission measurements of hollow-core THz Bragg fibers. JOSA B, 28(4), pp.896-907.

[2] Hong, B., Swithenbank, M., Greenall, N., Clarke, R.G., Chudpooti, N., Akkaraekthalin, P., Somjit, N., Cunningham, J.E. and Robertson, I.D., 2018. Low-Loss Asymptotically Single-Mode THz Bragg Fiber Fabricated by Digital Light Processing Rapid Prototyping. IEEE Transactions on Terahertz Science and Technology, 8(1), pp.90-99.

[3] Li, J., Nallappan, K., Guerboukha, H. and Skorobogatiy, M., 2017. 3D printed hollow core terahertz Bragg waveguides with defect layers for surface sensing applications. Optics Express, 25(4), pp.4126-4144.

[4] Wu, Z., Ng, W.R., Gehm, M.E. and Xin, H., 2011. Terahertz electromagnetic crystal waveguide fabricated by polymer jetting rapid prototyping. Optics express, 19(5), pp.3962-3972.

[5] Yang, J., Zhao, J., Gong, C., Tian, H., Sun, L., Chen, P., Lin, L. and Liu, W., 2016. 3D printed low-loss THz waveguide based on Kagome photonic crystal structure. Optics express, 24(20), pp.22454-22460.

[6]Setti, V., Vincetti, L. and Argyros, A., 2013. Flexible tube lattice fibers for terahertz applications. Optics express, 21(3), pp.3388-3399.

[7] Lu, W., Lou, S. and Argyros, A., 2016. Investigation of Flexible Low-Loss Hollow-Core Fibres With Tube-Lattice Cladding for Terahertz Radiation. IEEE Journal of Selected Topics in Quantum Electronics, 22(2), pp.214-220.

[8] Chen, D. and Chen, H., 2010. A novel low-loss Terahertz waveguide: Polymer tube. Optics express, 18(4), pp.3762-3767.

[9] Bao, H., Nielsen, K., Bang, O. and Jepsen, P.U., 2015. Dielectric tube waveguides with absorptive cladding for broadband, low-dispersion and low loss THz guiding. Scientific reports, 5, p.7620.

[10] Mitrofanov, O., James, R., Fernández, F.A., Mavrogordatos, T.K. and Harrington, J.A., 2011. Reducing transmission losses in hollow THz waveguides. IEEE Transactions on Terahertz Science and Technology, 1(1), pp.124-132.

[11] Navarro-Cía, M., Melzer, J.E., Harrington, J.A. and Mitrofanov, O., 2015. Silver-coated Teflon tubes for waveguiding at 1–2 THz. Journal of Infrared, Millimeter, and Terahertz Waves, 36(6), pp.542-555.

[12] Carmel, Y., Chu, K.R., Dialetis, D., Fliflet, A., Read, M.E., Kim, K.J., Arfin, B. and Granatstein, V.L., 1982. Mode competition, suppression, and efficiency enhancement in overmoded gyrotron oscillators. International Journal of Infrared and Millimeter Waves, 3(5), pp.645-665.

[13] Hong, B., Swithenbank, M., Somjit, N., Cunningham, J. and Robertson, I., 2016. Asymptotically single-mode small-core terahertz Bragg fibre with low loss and low dispersion. Journal of Physics D: Applied Physics, 50(4), p.045104.

[14]Zhang, Y. and Robertson, I.D., 2010. Analysis and design of Bragg fibers using a novel confinement loss diagram approach. Journal of Lightwave Technology, 28(22), pp.3197-3206.

[15] Johnson, S.G., Ibanescu, M., Skorobogatiy, M., Weisberg, O., Engeness, T.D., Soljačić, M., Jacobs, S.A., Joannopoulos, J.D. and Fink, Y., 2001. Low-loss asymptotically single-mode propagation in large-core OmniGuide fibers. Optics Express, 9(13), pp.748-779.

[16] Argyros, A., 2002. Guided modes and loss in Bragg fibres. Optics Express, 10(24), pp.1411-1417.

[17] Temelkuran, B., Hart, S.D., Benoit, G., Joannopoulos, J.D. and Fink, Y., 2002. Wavelength-scalable hollow optical fibres with large photonic bandgaps for CO2 laser transmission. Nature, 420(6916), pp.650-653.

[18] Siegel, P.H., 2004. Terahertz technology in biology and medicine. IEEE transactions on microwave theory and techniques, 52(10), pp.2438-2447.

[19] Cooper, K.B., Dengler, R.J., Llombart, N., Thomas, B., Chattopadhyay, G. and Siegel, P.H., 2011. THz imaging radar for standoff personnel screening. IEEE Transactions on Terahertz Science and Technology, 1(1), pp.169-182.

[20] Hong, B., Somjit, N., Cunningham, J. and Robertson, I., 2017, September. High-order operating mode selection using second-order bandgap in THz Bragg fiber. In Millimetre Waves and Terahertz Technologies (UCMMT), 2017 10th UK-Europe-China Workshop on (pp. 1-2). IEEE.

[21] Yeh, P., Yariv, A. and Marom, E., 1978. Theory of Bragg fiber. JOSA, 68(9), pp.1196-1201.

[22] Guo, S., Albin, S. and Rogowski, R.S., 2004. Comparative analysis of Bragg fibers. Optics express, 12(1), pp.198-207.

[23] Robertson, I., Somjit, N. and Chongcheawchamnan, M., 2016. Microwave and Millimetre-Wave Design for Wireless Communications. John Wiley & Sons.

[24]Roels, J., De Vlaminck, I., Lagae, L., Maes, B., Van Thourhout, D. and Baets, R., 2009. Tunable optical forces between

nanophotonic waveguides. Nature nanotechnology, 4(8), pp.510-513.
[25] Park, H.G., Huang, S.Y. and Kim, B.Y., 1989. All-optical intermodal switch using periodic coupling in a two-mode waveguide. Optics letters, 14(16), pp.877-879.
[26] Cohen, L.G. and Schneider, M.V., 1974. Microlenses for coupling junction lasers to optical fibers. Applied Optics, 13(1), pp.89-94.
[27] Vitiello, M.S., Xu, J.H., Kumar, M., Beltram, F., Tredicucci, A., Mitrofanov, O., Beere, H.E. and Ritchie, D.A., 2011. High efficiency coupling of Terahertz micro-ring quantum cascade lasers to the low-loss optical modes of hollow metallic waveguides. Optics express, 19(2), pp.1122-1130.
[28] Cregan, R.F., Mangan, B.J., Knight, J.C., Birks, T.A., Russell, P.S.J., Roberts, P.J. and Allan, D.C., 1999. Single-mode photonic band gap guidance of light in air. Science, 285(5433), pp.1537-1539.
[29] Knight, J.C., Birks, T.A., Russell, P.S.J. and Atkin, D.M., 1996. All-silica single-mode optical fiber with photonic crystal cladding. Optics letters, 21(19), pp.1547-1549.
[30] A. W. Snyder and J. D. Love, Optical Waveguide Theory (Chapman and Hall, 1983), Chap. 27
[31] Ito, T., Matsuura, Y., Miyagi, M., Minamide, H. and Ito, H., 2007. Flexible terahertz fiber optics with low bend-induced losses. JOSA B, 24(5), pp.1230-123
[32] Layton, M.R. and Bucaro, J.A., 1979. Optical fiber acoustic sensor utilizing mode-mode interference. Applied Optics, 18(5), pp.666-670.
[33] B. Hong et al., "Data associated with 'Investigation of Electromagnetic Mode Transition and Filtering of Asymptotically Single-mode Hollow THz Bragg Fibre'," Univ. Leeds, Leeds, U.K., 2017. [Online]. Available: https://doi.org/10.5518/248